International Journal of Bifurcation and Chaos, Vol. 11, No. 7 (2001) 1911–1927

BIFURCATION ANALYSIS OF A PWL CHAOTIC CIRCUIT BASED ON HYSTERESIS THROUGH A ONE-DIMENSIONAL MAP

FEDERICO BIZZARRI and MARCO STORACE
Department of Biophysical and Electronic Engineering, University of Genoa, Via Opera Pia 11a, I-16145 Genova, Italy

LAURA GARDINI
Department of Economic Sciences, University of Urbino, Via A. Saffi 2, I-61029 Urbino, Italy

RENZO LUPINI
Department of Mathematics, University of Ancona, Via Brecce Bianche, I-60131 Ancona, Italy

Received August 23, 2000; Revised September 15, 2000

Bifurcations in the dynamics of a chaotic circuit based on hysteresis are evaluated. Owing to the piecewise-linear nature of the nonlinear elements of the circuit, such bifurcations are discussed by resorting to a suitable one-dimensional map. As the ordinary differential equations governing the circuit are piecewise linear, the analytical expressions of their solutions can be derived in each linear region. Consequently, the proposed results have been obtained not by resorting to numerical integration, but by properly connecting pieces of planar flows. The bifurcation analysis is carried out by varying one of the three dimensionless parameters that the system of normalized circuit equations depends on. Local and global bifurcations, regular and chaotic asymptotic behaviors are pointed out by analyzing both the one-dimensional map and the three-dimensional flow induced by the circuit dynamics.

1. Introduction

This paper deals with the dynamics of a recently proposed chaotic circuit based on hysteresis [Storace & Parodi, 1998; Storace *et al.*, 1999].

Under a specific hypothesis on the circuit parameters, the three-dimensional flow corresponding to the system of normalized circuit equations turns out to be piecewise linear (PWL). However, in contrast with common invertible three-dimensional flows (giving rise to invertible two-dimensional return-maps), it can be studied through a suitable one-dimensional map denoted by g.

As the flow is noninvertible and noncontinuous with respect to the initial conditions, the map g is, in turn, noninvertible and can exhibit both discontinuities and lack of smoothness. Unlike what occurs in several continuous models, in the proposed system many of the properties of the map g can be analytically proved, among which the ranges of continuity and the appearance/disappearance of discontinuities [Lupini *et al.*, 2001].

Through the map g, many dynamic features of the flow can be ultimately described, such as local and global bifurcations, regular or chaotic asymptotic behavior. The tangent (or fold) bifurcations of g or of its kth iteration g^k ($k > 1$) are related to the existence of limit cycles in the flow. It can also be shown that the predominant regime is chaotic. In other words, an attracting region in the state space exists from which the trajectories cannot escape,

inside which the generic behavior is aperiodic, wandering unpredictably among infinite unstable limit cycles of the flow. A particularly important global bifurcation, which can be completely characterized in the three-dimensional parameter space, marks the transition from a bistable regime to a single attractor. In the bistable case, there are two coexisting symmetric attractors, generally chaotic, whose basins are separated by the stable manifold of a particular unstable cycle in the flow. The transition to a single attractor occurs when the stable manifold of the cycle belonging to the basin boundary has a contact with its unstable manifold, causing a homoclinic tangle. This is simply proved through the map g by detecting the first homoclinic bifurcation of one of its fixed points.

The circuit is described in Sec. 2. After deriving a set of normalized equations describing the dynamics of the circuit, the main features of the flow (i.e. equilibrium points and qualitative behaviors of the trajectories) are pointed out.

In Sec. 3, we show that the three-dimensional dynamics of the circuit can be captured by a one-dimensional map, g. Some basic properties of the map g are discussed.

Section 4 is devoted to the description of the main bifurcations occurring in the flow when one of the system parameters is varied. Such a description is supported by the analysis of the changes in the map g, which undergoes the same type of bifurcations as the flow.

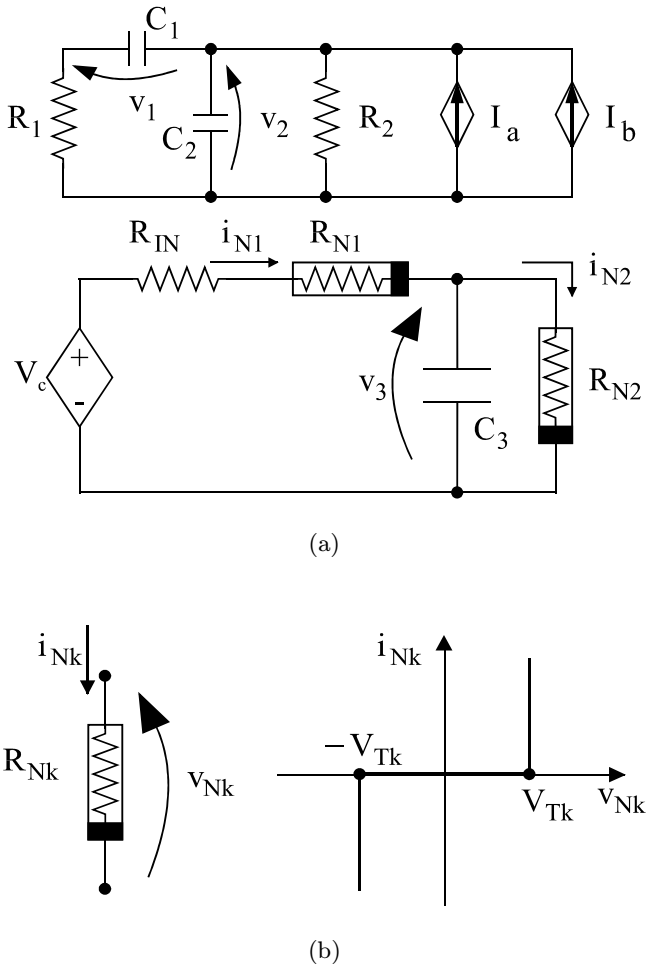

Fig. 1. (a) The chaotic circuit and (b) the PWL driving-point characteristics of its nonlinear resistors.

2. The Circuit and its Mathematical Model

The considered circuit is made up of a linear part and a hysteretic cell, as shown in Fig. 1(a) (upper and lower parts, respectively).

The linear part is identical to that of the circuit proposed in [Nakagawa & Saito, 1996]. It contains two linear resistors, R_1 and R_2, two linear capacitors, C_1 and C_2 (corresponding to the state variables v_1 and v_2), and two linear voltage-controlled current sources, $I_a(v_1, v_2) = G_a(v_1 + v_2)$ and $I_b(v_3) = -G_b v_3$, where G_a and G_b are positive coefficients $[\Omega^{-1}]$.

The hysteretic cell is based on the circuit model of hysteresis proposed by Parodi *et al.* [1994, 1996]. It contains a linear resistor, R_{IN}, a linear capacitor, C_3 (corresponding to the state variable v_3), two nonlinear resistors, R_{N1} and R_{N2}, and a linear voltage-controlled voltage source, $V_c(v_1) = v_1$.

The two parts of the circuit interact through the three linear controlled sources $I_a(v_1, v_2)$, $I_b(v_3)$ and $V_c(v_1)$.

The equation governing the hysteretic cell is

$$C_3 \frac{dv_3}{dt} = i_{N1}(v_{N1}) - i_{N2}(v_{N2})\,. \tag{1}$$

The PWL driving point (DP) characteristics $i_{Nk}(v_{Nk})$ of the nonlinear resistors are shown in Fig. 1(b).

By defining

$$\rho(x) = x - \frac{|x+1| - |x-1|}{2} \tag{2}$$

and considering the series combination of R_{IN} and R_{N1}, we can express the current i_{N1} in terms of the voltage $v_1 - v_3$ as follows:

$$i_{N1}(v_1, v_3) = \frac{V_{T1}}{R_{IN}} \rho\left(\frac{v_1 - v_3}{V_{T1}}\right)\,. \tag{3}$$

By doing so, we can obtain the canonical form of the nonlinear state equations for the whole circuit:

$$\begin{aligned} C_1\frac{dv_1}{dt} &= -\frac{1}{R_1}(v_1+v_2) \\ C_2\frac{dv_2}{dt} &= -\frac{1}{R_1}(v_1+v_2)-\frac{1}{R_2}v_2 \\ &\quad +G_a(v_1+v_2)-G_bv_3 \\ C_3\frac{dv_3}{dt} &= i_{N1}(v_1,\,v_3)-i_{N2}(v_3)\,. \end{aligned} \tag{4}$$

For the sake of simplicity, in the following we shall assume $C_1 = C_2 = C_3 = C$ and $R_1 = R_2 = R$.

Under the hypothesis of rate-independence [Parodi *et al.*, 1994, 1996],

$$R_{IN} \ll \frac{1}{\Omega C_3} \tag{5}$$

where Ω is the highest angular frequency in the spectrum of v_1 [Storace & Parodi, 1998], the nonlinear differential equation governing the hysteretic cell turns out to generate the v_3 versus v_1 PWL hysteresis relationship shown in Fig. 2.

Figure 2 points out the fundamental difference with respect to the hysteretic cell considered in [Nakagawa & Saito, 1996]. As a matter of fact, such a cell generates a sort of Schmitt-trigger cycle by resorting to the "jump phenomenon" described in [Kennedy & Chua, 1991]. Then, in contrast with the cell considered in this paper, it does not allow the trajectories to reach points like F and H in Fig. 2. Moreover, all the points that lie within the cycle in Fig. 2 can be reached by the flow, according to the local memory property of the hysteresis cycle (i.e. only by horizontal motion, as for the point E) [Parodi *et al.*, 1994; Storace *et al.*, 1999].

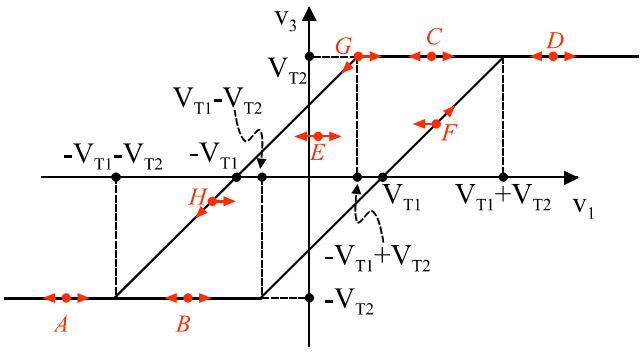

Fig. 2. The v_3 versus v_1 hysteresis cycle and the possible evolutions of the trajectories on the (v_1, v_3) plane for all different kinds of reachable points A–H.

We now introduce the normalized variables

$$\tau = \frac{t}{RC}\,; \quad x = \frac{v_1}{V_{T1}}\,; \quad y = \frac{dx}{d\tau} = \dot{x}\,; \quad z = \frac{v_3}{V_{T2}} \tag{6}$$

and the normalized parameters

$$q = \frac{V_{T2}}{V_{T1}}\,; \quad p = \frac{RG_bV_{T2}}{V_{T1}}\,; \quad \delta = \frac{(G_aR-3)}{2}\,. \tag{7}$$

The hysteretic behavior displayed in Fig. 2 does not depend on the value of R_{IN}, provided that the rate-independence inequality (5) holds. Consequently,

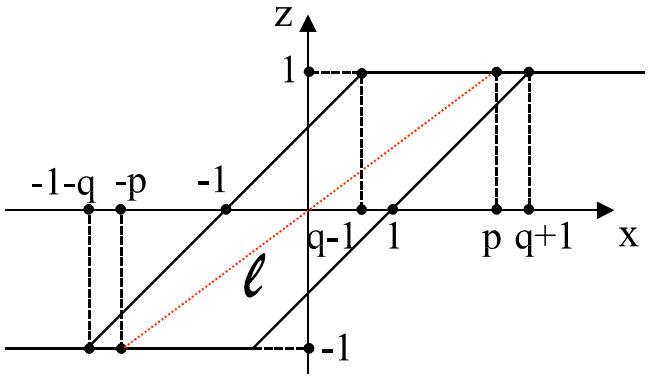

(a)

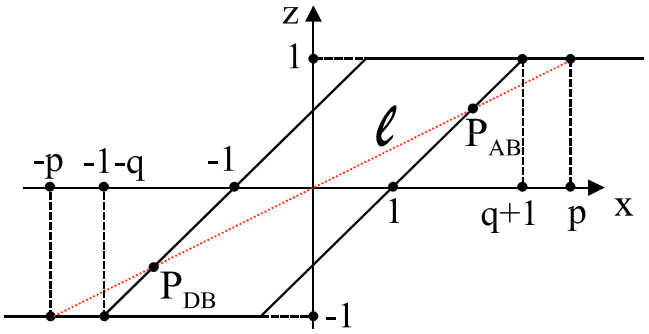

(b)

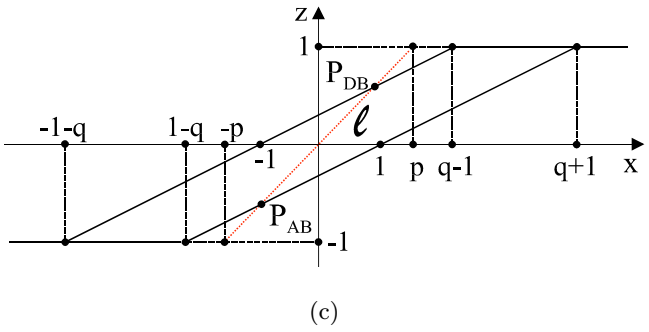

(c)

Fig. 3. Examples of hysteretic relationships between z and x for (a) $q-1 < p < q+1$, (b) $p > q+1$ and (c) $p < q-1$.

we obtain a three-dimensional PWL flow made up of planar pieces, each being governed (in the normalized space (x, y, z)) by a linear system of two first-order differential equations:

$$\begin{aligned} \dot{x} &= y \\ \dot{y} &= 2\delta y - x + pz \end{aligned} \tag{8}$$

Note that:

(i) the quote z depends on both the initial conditions and the variable x via the hysteresis relationship shown in Fig. 3;
(ii) the transitions between different planar pieces of flow (corresponding to different expressions for the quote $z(x)$) are governed by a proper set of switching rules (imposed by the hysteretic nonlinearity), which are briefly described here (and illustrated in greater detail in the next section).

The planar pieces of the flow lie on the following surfaces, schematically represented in Fig. 4:

$S_{DB} = \{(x, y, z) : -1 - q \le x \le -1 + q, z = (x + 1)/q\}$
$S_{AB} = \{(x, y, z) : 1 - q \le x \le 1 + q, z = (x - 1)/q\}$
$S_+ = \{(x, y, z) : x \ge -1 + q, z = 1\}$
$S_- = \{(x, y, z) : x \le 1 - q, z = -1\}$
$S_h = \{(x, y, z) : -1 + hq \le x \le 1 + hq, z = h\}$, $h \in (-1, 1)$

The equations governing the dynamics on the horizontal surfaces $S_+(h = 1)$, $S_-(h = -1)$ and $S_h(h \in (-1, 1))$ are

$$\begin{aligned} \dot{x} &= y \\ \dot{y} &= 2\delta y - x + ph \end{aligned} \tag{9}$$

whereas, on the oblique surfaces S_{DB} and S_{AB}, the flow obeys the equations

$$\begin{aligned} \dot{x} &= y \\ \dot{y} &= 2\delta y - x + p\frac{x \pm 1}{q} \end{aligned} \tag{10}$$

The pieces of planar flow are connected to each other with continuity along particular curves where the switching rules apply:

- a trajectory on a surface S_h enters one of the oblique surfaces (S_{DB} or S_{AB}) as soon as it intersects it;
- on the surface S_+ (or S_-), a trajectory changes flow when it reaches S_{DB} (or S_{AB});
- on S_{DB} (or S_{AB}), a trajectory enters either a surface S_h, as soon as it intersects the plane $y = 0$, or the surface S_- (or S_+), as soon as it intersects the plane $z = -1$ (or $z = +1$).

The equilibrium points of the system turn out to be the following:

$P_{S\pm} = (\pm p, 0, \pm 1)$	on $S_\pm$
$P_h = (hp, 0, h)$	on S_h
$P_{DB} = (-p/(p - q), 0, -1/(p - q))$	on S_{DB}
$P_{AB} = -P_{DB}$	on S_{AB}

The hysteresis cycles shown in Fig. 3 point out the geometrical meanings of the positive parameters q and p; $1/q$ is the slope of the ascending and descending branches of the hysteresis cycle, and $1/p$ is the slope of the locus ℓ of the equilibrium points lying on S_+, S_- and S_h. It is worth noting that, for $q - 1 < p < q + 1$, ℓ lies completely within the hysteresis cycle, as in Fig. 3(a), whereas, for $p \ge q + 1$ and $p \le q - 1$, a part of ℓ lies outside the cycle, as shown in Figs. 3(b) and 3(c), respectively. Of course, the equilibrium points lying outside the hysteresis cycle are virtual. For $p \ge q+1$ and $p \le q-1$, the two symmetric equilibrium points P_{DB} and P_{AB} belong both to S_h (where $h = -1/(p - q)$ for P_{DB} and $h = 1/(p - q)$ for P_{AB}) and to either S_{DB} or S_{AB}, respectively.

The eigenvalues of the Jacobian matrices evaluated at the equilibrium points $P_{S\pm}$ and P_h are

$$\lambda_\pm = \delta \pm \sqrt{\delta^2 - 1}\,. \tag{11}$$

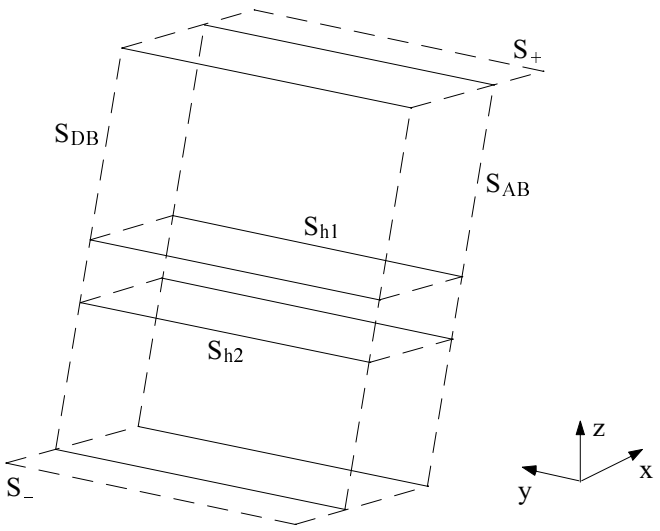

Fig. 4. The planar surfaces in the phase space.

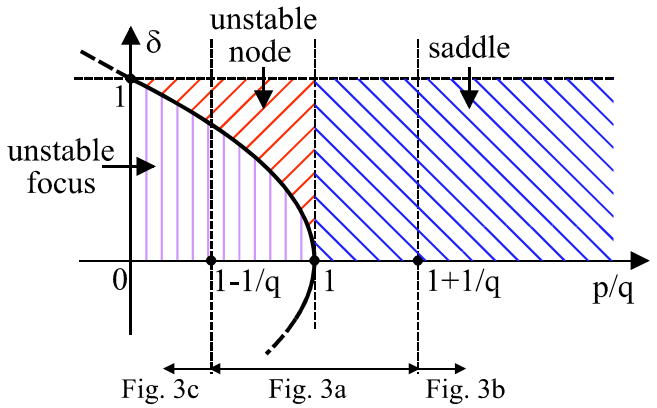

Fig. 5. Diagram showing the type and the stability of the fixed points. The equation for the parabola (bold line) is $\delta^2 - 1 + p/q = 0$.

Henceforth we shall assume $\delta \in (0, 1)$ (hence $P_{S\pm}$ and P_h are unstable foci).

The eigenvalues of the Jacobian matrices evaluated at the equilibrium points P_{DB} and P_{AB} are

$$\lambda_\pm = \delta \pm \sqrt{\delta^2 - 1 + \frac{p}{q}}\,. \qquad (12)$$

Figure 5 shows the nature of the equilibrium points on S_{DB} and S_{AB} as a function of $\delta(\in (0, 1))$ and p/q. The correspondences between the parameter values and the hysteresis cycles in Fig. 3 are pointed out (bottom of Fig. 5).

To sum up, the rules for the flow imposed by the hysteretic cell are such that, on the boundary surfaces (S_+, S_-, S_{DB} and S_{AB}) and on the inner horizontal surfaces (S_h), the flow results from the union of linear, planar pieces, each of which is described by Eq. (8) with the proper expression for the quote z [i.e. by either Eq. (9) or (10)]. Switching between different pieces of flow occurs when the trajectories cross particular lines at the intersection between boundary surfaces [see the black dots in Fig. 6(a)]. We define two particular lines:

- the intersection of S_{DB} with the plane $y = 0$, i.e. the locus γ_A of the transition points from S_{DB} to the horizontal surfaces S_h;
- the intersection of S_{DB} with S_- in the range $y \leq 0$, i.e. the locus γ_B of the transition points from S_{DB} to S_-.

Both γ_A and γ_B are shown in Fig. 6(a). Owing to the symmetry of the three-dimensional system (1), the switching rules for the flow are symmetric with respect to the origin.

As we shall see in the following sections, because of such switches, the resulting flow turns out to be nonsmooth, noninvertible and even discontinuous for most parameter values, as a function of the initial conditions.

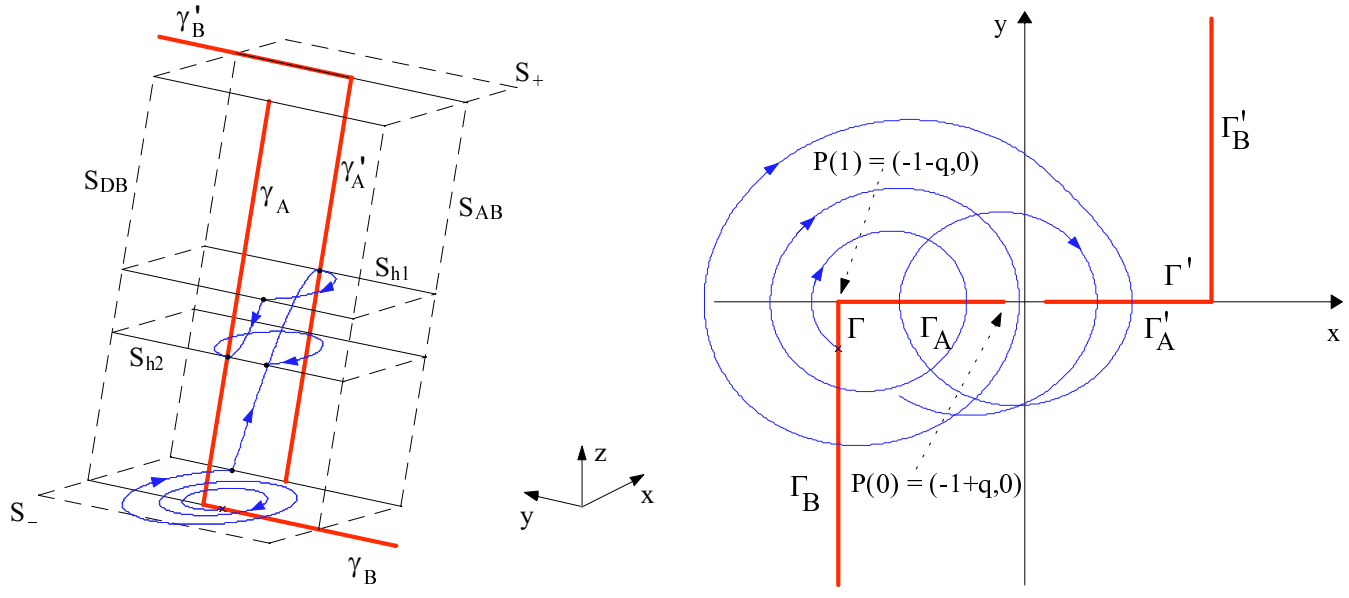

Fig. 6. (a) Example of trajectory in the (x, y, z) space and (b) its projection on the (x, y) plane.

3. The 1-D Map g

In this section, we shall show that the three-dimensional flow described in the previous section gives rise to a flow with a nonunique inverse whose asymptotic dynamics is reflected in a one-dimensional, noninvertible map.

To this end, we consider the projections (on the (x, y) plane) of the three-dimensional trajectories [see Fig. 6(b), which corresponds to Fig. 6(a)] representing the motion of the plane linear oscillator described by Eq. (8) and by proper switching lines related to the hysteretic relationship between z and x, as defined in Sec. 2.

3.1. *The curve* Γ

The piecewise-linear curve Γ is made up of the segment Γ_A and the half-line Γ_B, Γ_A and Γ_B being the projections of γ_A and γ_B on the (x, y) plane, respectively.

Henceforth, we will focus our attention on Γ and its symmetric Γ' with respect to the origin [Fig. 6(b)]. In the following, the symmetric figure (with respect to the origin) of any figure F will be denoted by F'.

Γ can be parameterized by introducing the variable $\xi \in [0, +\infty)$ related to x and y as follows:

$$\xi = \begin{cases} -\dfrac{x+1-q}{2q} & \text{for } x \in (-1-q,\, -1+q] \\ & \text{(i.e. on } \Gamma_A\text{)} \\ 1-y & \text{for } x = -1-q,\ y \le 0 \\ & \text{(i.e. on } \Gamma_B\text{)} \end{cases} \tag{13}$$

Note that $\xi = 1$ corresponds to the vertex of Γ.

As outlined in Figs. 2 and 3, z is related to x on Γ as follows:

$$z = \frac{x+1}{q} \quad \text{on } \Gamma_A\,; \quad z = -1 \quad \text{on } \Gamma_B \tag{14}$$

As Γ' and Γ are symmetric with respect to the origin, Γ' inherits a similar parameterization. In other words, Γ' is parameterized by ξ' as follows ($\xi' = 1$ corresponds to the vertex of Γ'):

$$\xi' = \begin{cases} -\dfrac{-x+1-q}{2q} & \text{for } x \in (1-q,\, 1+q) \\ & \text{(i.e. on } \Gamma'_A\text{)} \\ 1+y & \text{for } x = 1+q,\ y \ge 0 \\ & \text{(i.e. on } \Gamma'_B\text{)} \end{cases} \tag{15}$$

Note that two different points defined by the same value of ξ and ξ' are symmetric.

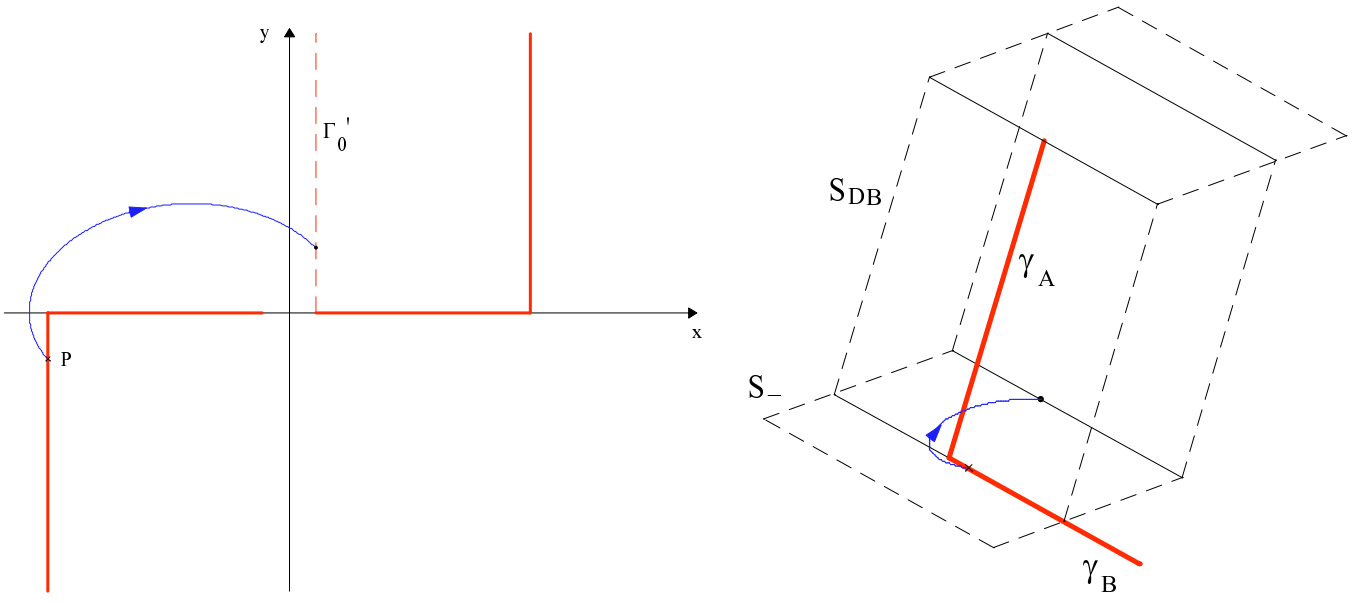

(a) (b)

Fig. 7. Example of switching rule 1.

In the following, the relationship between a point $P = (x, y)$ on Γ and the corresponding value of ξ will be labeled by the notation $P(\xi)$ (*vice versa*, the value of ξ corresponding to P will be denoted by $\xi(P)$). A trajectory with an initial point P, associated with the considered system of equations and with its switching rules, is denoted by $\varphi(P, t)$.

3.2. *Switching lines and switching rules*

According to this new parameterization, the switching rules described in the previous section lead to the definition of two families of switching lines, i.e. the set of half-lines Γ_ξ, originating in $P(\xi)$ ($\xi \in [0, 1]$) and parallel to Γ_B, and the symmetric set Γ'_ξ. The half-line corresponding to the vertex of Γ (i.e. Γ_1) coincides with Γ_B.

The switching rules for the linear pieces of $\varphi(P, t)$ issuing from Γ and from the half-lines Γ_ξ turn out to be the following:

(1) For an initial condition $P = (x_0, y_0) \in \Gamma_B$, z is equal to -1. Then, assuming $\delta \in (0, 1)$, $\varphi(P, t)$ is an expanding spiral centred at $(-p, 0)$ (see Fig. 7). The subsequent switch occurs when the trajectory arrives on Γ'_0. In the three-dimensional model, this piece of trajectory corresponds to the motion on S_-, as shown in Fig. 7(b).

(2) For an initial condition $P = (x_0, 0) \in \Gamma_A$, we have $\xi(P) = -((1 - q + x_0)/2q)$, and z is equal to $z_0 = (x_0 + 1)/q$.

For $p \leq q - 1$, the subsequent switch occurs when

(2.a1) either $\varphi(P, t)$ (for $x_0 < -(p/(p - q))$, i.e. for $\xi(P) > (p - q + 1)/2(p - q)$) arrives on $\Gamma'_{1-\xi}$, as shown in Fig. 8(a) (blue line starting from P_1)

(2.a2) or $\varphi(P, t)$ (for $x_0 < -(p/(p - q))$) returns to Γ_ξ, as shown in Fig. 8(a) (green line starting from P_2)

(2.a3) or $\varphi(P, t)$ (for $x_0 > -(p/(p-q))$) arrives on Γ_B, as shown in Fig. 8(a) (green line starting from P_3)

(2.a4) or $\varphi(P, t)$ (for $x_0 > -(p/(p - q))$) arrives on Γ_{ξ^*} ($\xi^* > \xi(P)$), as shown in Fig. 8(a) (blue line starting from P_3).

In the three-dimensional model, the first two pieces of trajectories correspond to divergent ($\delta \in (0, 1)$) spiral motions on S_h ($h = z_0$) [see Fig. 8(b)], whereas the other two pieces of trajectory correspond to divergent motions on S_{DB} [see Fig. 8(b)].

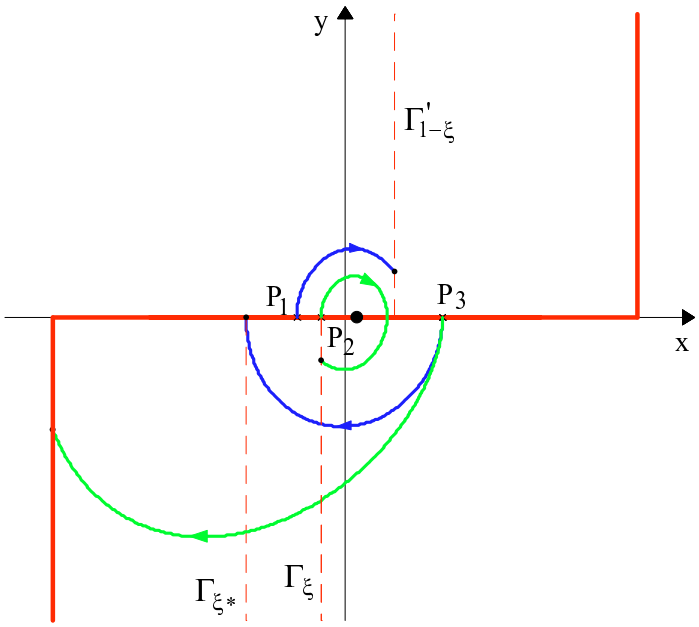

(a)

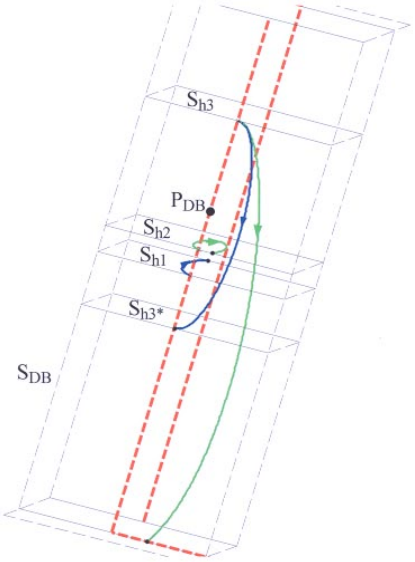

(b)

Fig. 8. Examples of switching rules (2.a1)–(2.a4).

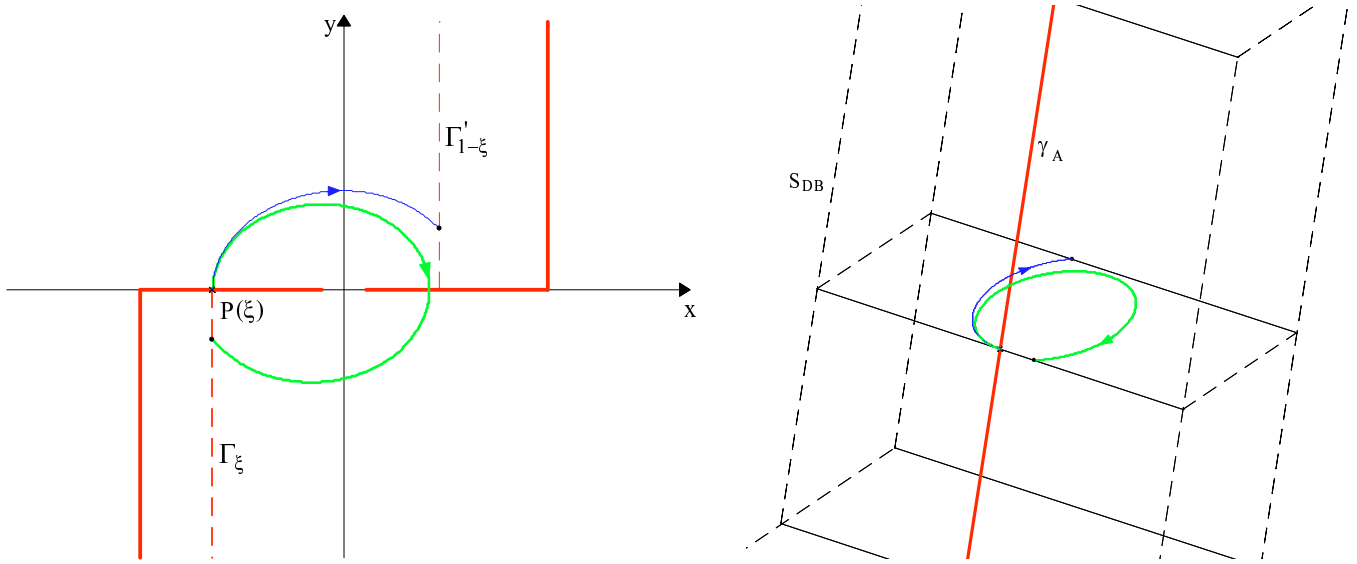

(a) (b)

Fig. 9. Examples of switching rules (2.b1) and (2.b2).

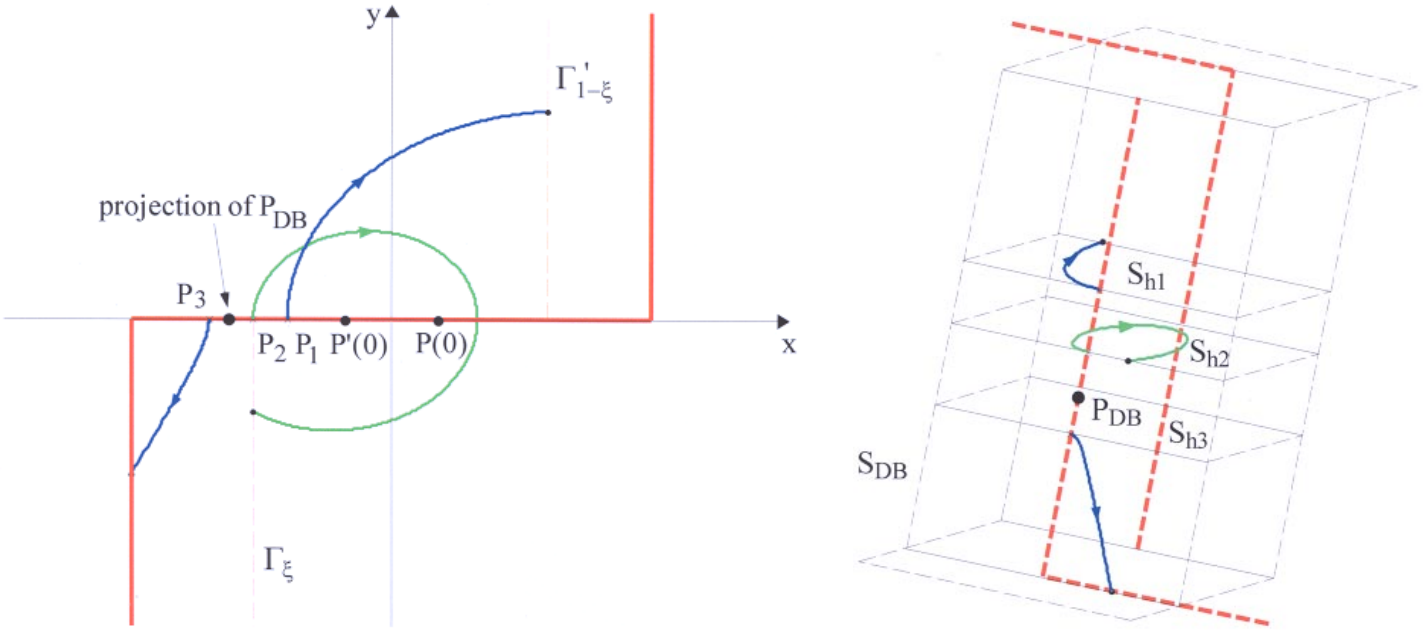

(a) (b)

Fig. 10. Examples of switching rules (2.c1)–(2.c3).

For $q-1 < p < q+1$, the subsequent switch occurs when

(2.b1) either $\varphi(P, t)$ arrives on $\Gamma'_{1-\xi}$, as shown in Fig. 9(a) (blue line)

(2.b2) or $\varphi(P, t)$ returns to Γ_ξ, as shown in Fig. 9(a) (green line).

In the three-dimensional model, such pieces of trajectories correspond to divergent spiral motions on S_h ($h = z_0$) [see Fig. 9(b)].

(3) For $p \geq q + 1$, the subsequent switch occurs when

(2.c1) either $\varphi(P, t)$ (for $x_0 > -(p/(p - q))$,

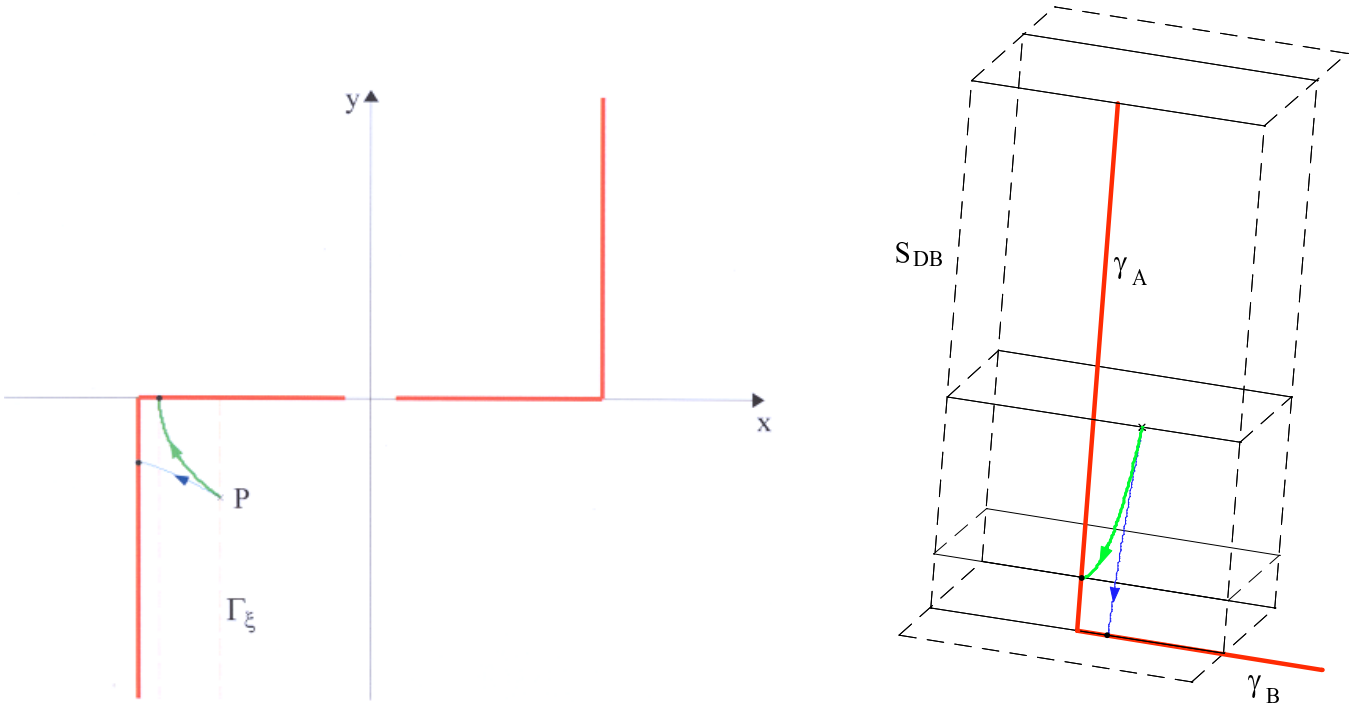

(a) (b)

Fig. 11. Examples of switching rules (3.a) and (3.b).

i.e. for $\xi(P) < (p-q+1)/2(p-q)$) arrives on $\Gamma'_{1-\xi}$, as shown in Fig. 10(a) (blue line starting from P_1)

(2.c2) or $\varphi(P, t)$ (for $x_0 > -(p/(p-q))$) returns to Γ_ξ, as shown in Fig. 10(a) (green line starting from P_2)

(2.c3) or $\varphi(P, t)$ (for $x_0 < -(p/(p-q))$) arrives on Γ_B, as shown in Fig. 10(a) (blue line starting from P_3).

In the three-dimensional model, the first two pieces of trajectories correspond to divergent spiral motions on S_h ($h = z_0$) [see Fig. 10(b)], whereas the third piece of trajectory corresponds to divergent motion on S_{DB} [see Fig. 10(b)].

(3) For an initial condition $P = (x_0, y_0) \in \Gamma_\xi$, z is equal to $z_0 = (x_0 + 1)/q$. For any values of p and q, the next switch occurs when $\varphi(P, t)$ arrives on Γ, on

(3.a) either Γ_A [green line in Fig. 11(a)]
(3.b) or Γ_B [blue line in Fig. 11(a)].

In the three-dimensional flow, such pieces of trajectories correspond to descents on S_{DB} connecting motions on horizontal planes [Fig. 11(b)].

These switching rules are completed by the symmetric ones of (1)–(3) with respect to the origin. Then, the flowchart of the switches of the trajectories can be summarized as shown in Fig. 12.

3.3. *The map g*

The dynamic process described above is uniquely defined for the future, but we may have discontinuities with respect to the initial conditions along particular trajectories (called *singular trajectories*) introduced in [Lupini *et al.*, 2001]. Even in the absence of singular trajectories, the above process in general defines only one (possibly discontinuous) flow for the future because invertibility may not be obeyed. An example is given in Fig. 13, where two different initial conditions, P_1 and P_2, are shown whose trajectories reach the same point P_3.

As we shall see below, this is just the reason why the considered dynamic system may exhibit the behavior complexity typical for one-dimensional noninvertible maps.

From the previous description of the switches, it follows that, for $1-q < p < 1+q$, trajectories starting from points of Γ will reach the symmetric curve Γ' in a finite time. The same holds for $p \leq 1 - q$

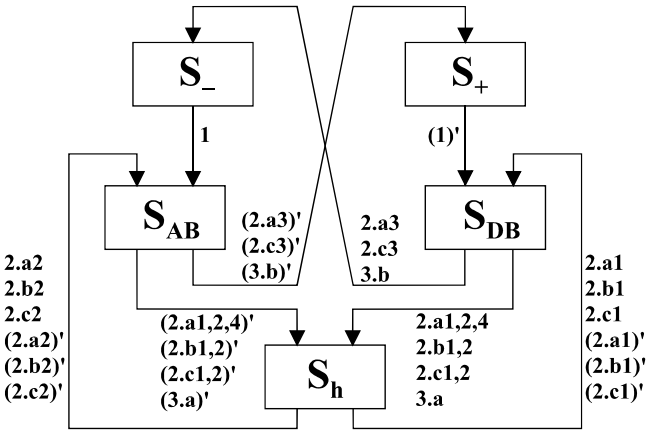

Fig. 12. Summary of the possible transitions with the corresponding switching rules (the notation (#)' stands for the switching rule symmetric to #).

and $p \geq 1+q$, provided that the starting point does not coincide with the (unstable) equilibrium point P_{DB}. Through the scalar parameterizations of the curves Γ and Γ', we can define the one-dimensional map that captures the asymptotic dynamics of the normalized circuit model as follows

$$\xi \to g(\xi)$$

$P'(g(\xi))$ being the first point of Γ' that will be visited by $\varphi(P(\xi), t)$ in the future. The map exhibits discontinuities for the set of values of ξ such that $P(\xi)$ belongs to singular trajectories. Moreover, g inherits lack of smoothness at $\xi = 1$ and for the set $\{g^{-1}(1)\}$ (set of rank-1 preimages of 1) from the lack of smoothness of the curves Γ and Γ' at $P(1)$ and $P'(1)$, respectively.

In particular, as the trajectory issuing from $P(1)$ is tangent to Γ_B, it follows that the derivative of g at $\xi = 1$ from the right is zero (i.e. $g'(1^+) = 0$). Analogously, as any trajectory arriving at $P'(1)$ is tangent to Γ'_B, at any $\xi \in \{g^{-1}(1)\}$ one of the one-sided derivatives of g is infinite.

We point out that, because of symmetry, $g^{(2)}$ is the first return map on Γ *after visiting* Γ'. The full dependence of the map g on the system's variables (i.e. the state variable ξ and the parameters p, q and δ) will be denoted by $g(\xi; p, q, \delta)$.

The seemingly contradictory result of a 1-D return map associated with a three-dimensional flow can be ascribed [Strogatz, 1994; Alligood & Sauer, 1997] to the noninvertibility of the flow, as noted above.

We remark that there exists a relationship between invariant sets in the map g and in the flow. To fixed points of g (stable or unstable) there correspond symmetric periodic orbits in the flow. On the other hand, to each fixed point of g^k $(k > 1)$, which is not a fixed point of g, there corresponds a nonsymmetric periodic orbit of the flow (hence the symmetric one exists, too). As an example,

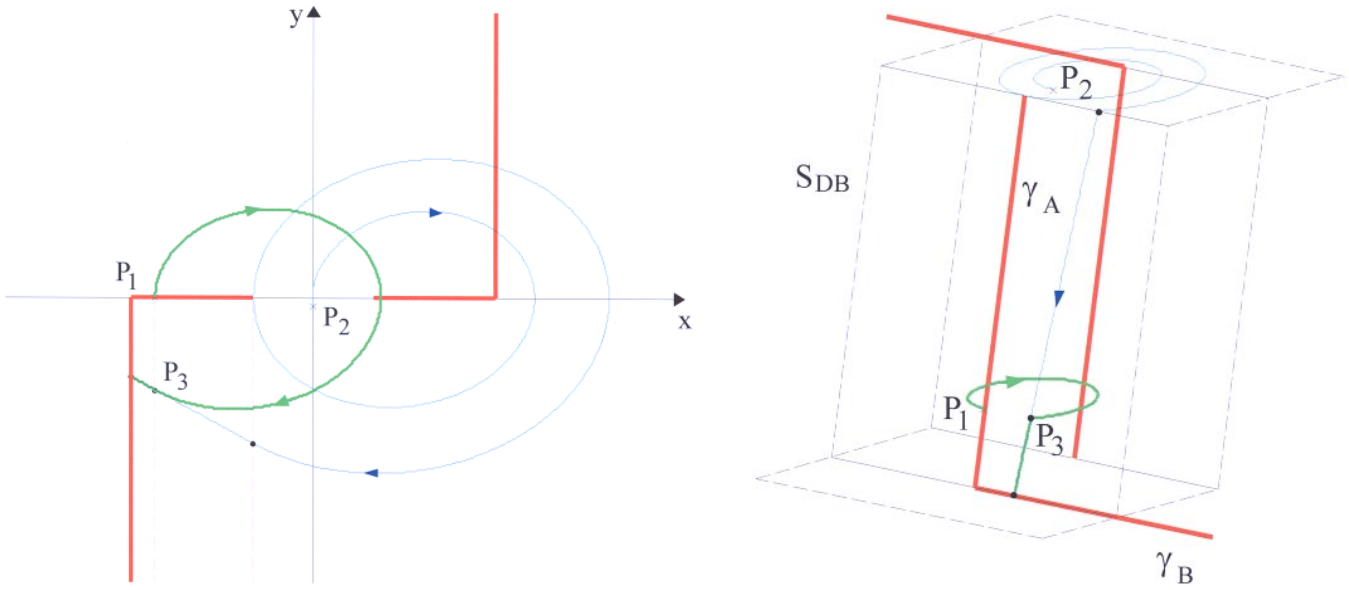

(a) (b)

Fig. 13. Example illustrating the noninvertibility of the flow.

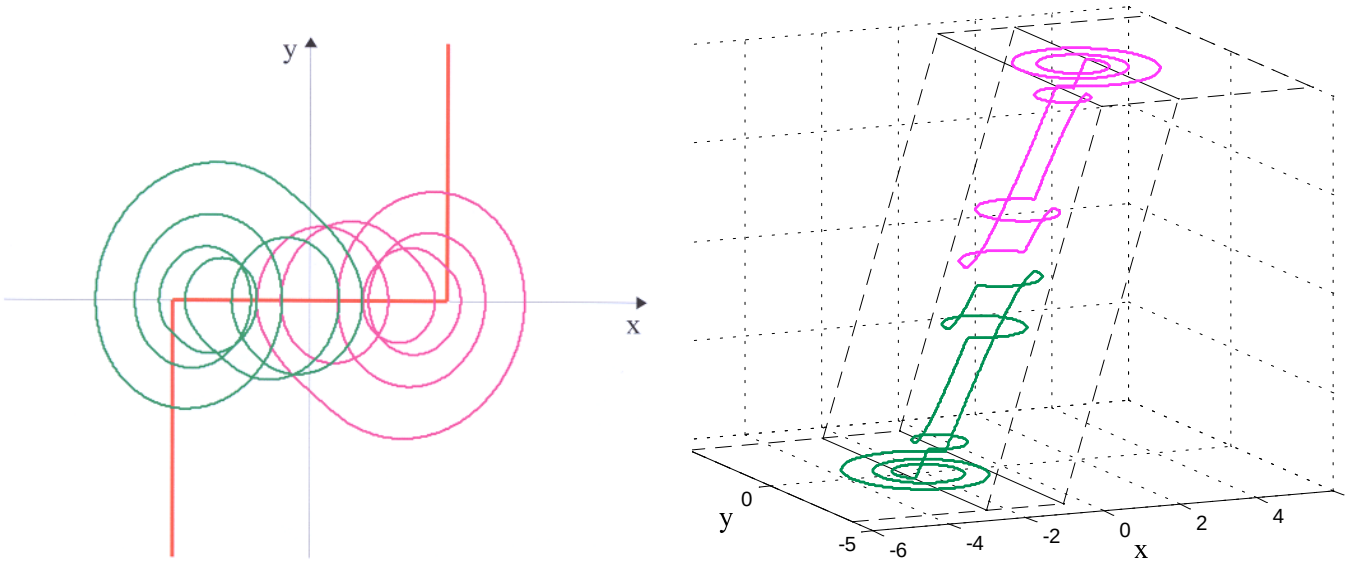

(a) (b)

Fig. 14. Example of a symmetric pair of (unstable) cycles for $p = 2$ (a) on the (x, y) plane and (b) in the (x, y, z) space.

for $p = 2$, two nonsymmetric unstable limit cycles, corresponding to a pair (abscissas $\xi \cong 0.48$ and $\xi \cong 0.64$) of repelling fixed points of g^2 (two-cycle of g), are shown in Fig. 14.

4. Global Dynamics

Generally speaking, we are interested in the study of bifurcations in the dynamics of the circuit when we vary the three parameters δ, p and q. In this paper, for the sake of simplicity, we report results for fixed values of δ and q (i.e. $\delta = 0.075$ and $q = 1.5$), whereas p is varied, i.e. we consider g as a one-parameter family of maps $g(\xi; p)$.

As p increases from 0, the trajectories of the flow are all divergent, except for the segment of (unstable) equilibrium points $x = pz$, $y = 0$. A bounded observable dynamics suddenly appears

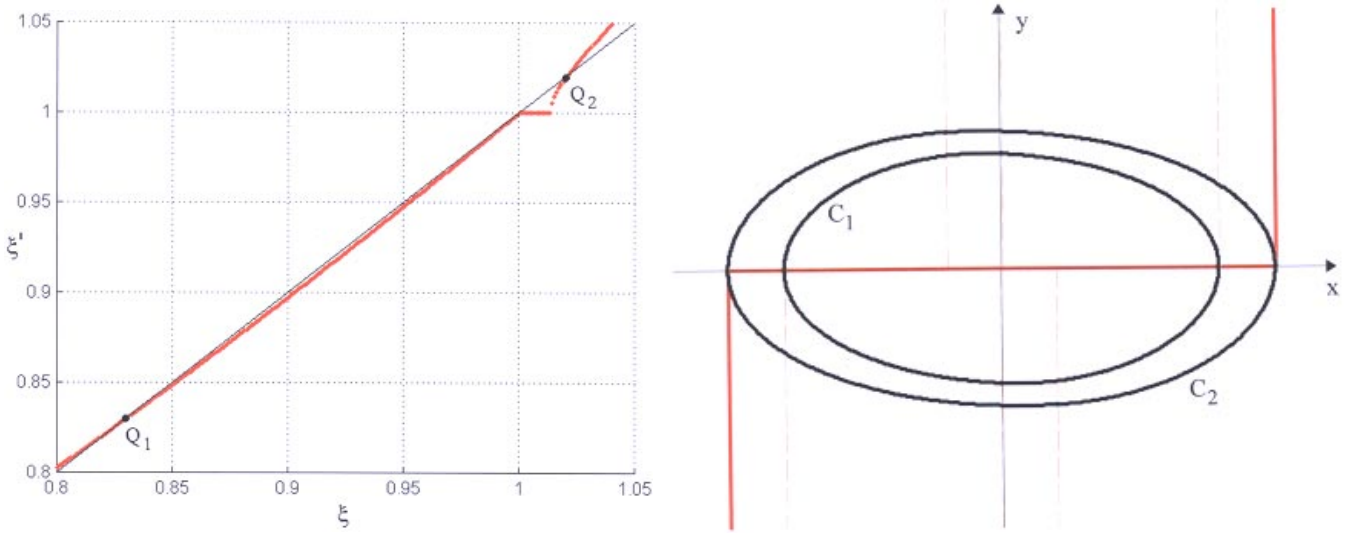

(a) (b)

Fig. 15. (a) Map g for $p = 0.63$; symmetric limit cycles C_1 (stable) and C_2 (unstable) corresponding to the fixed points Q_1 and Q_2 of g, respectively, (b) on the (x, y) plane and (c) in the (x, y, z) space.

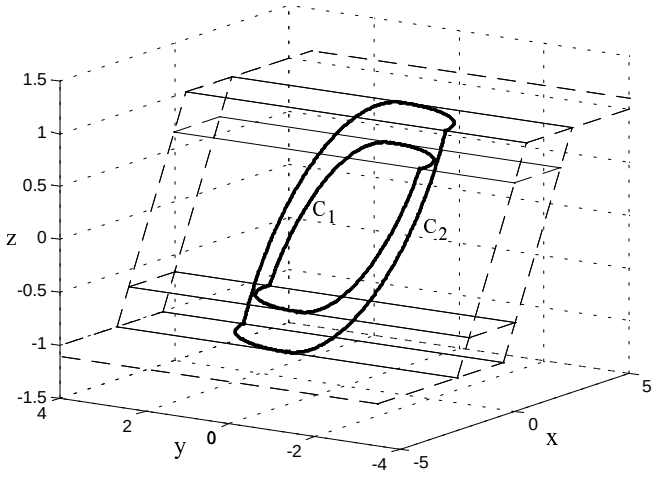

(c)

Fig. 15. (*Continued*)

at a bifurcation value $p = p_1 \cong 0.62$, for which a stable limit cycle is generated (C_1 in Fig. 15). All the trajectories (except for those originating in the equilibrium points) are either divergent or convergent to C_1. This is due to a kind of saddle-node bifurcation, which creates a couple of limit cycles, C_1 (stable) and C_2 (unstable). The stable manifold of C_2 separates divergent trajectories from eventually periodic trajectories.

We can easily see that, for small values of p, the map g, which reflects the properties of the flow, has no fixed points (its graph being located above the bisectrix line). An example is given in Fig. 16 ($p = 0.2$), where $g(\xi; p) > \xi$, $\forall \xi > 0$, and all the trajectories are divergent.

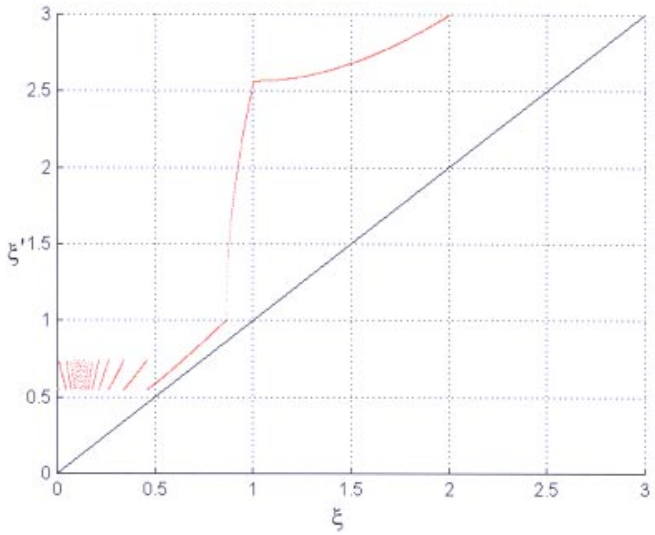

Fig. 16. The map g for $p = 0.2$.

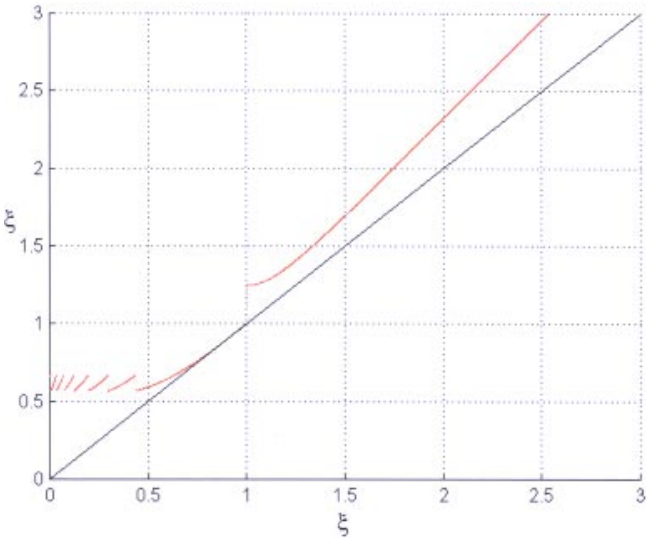

Fig. 17. The map g for $p = 0.62$ (near the contact bifurcation).

As p increases, the graph of g approaches the bisectrix line, and a "contact bifurcation" (or tangent bifurcation) occurs for $p = p_1$, as shown in Fig. 17. This bifurcation generates a pair of fixed points, one attracting, $Q_1 = (\xi_{Q1}, g(\xi_{Q1}))$, and the other repelling, $Q_2 = (\xi_{Q2}, g(\xi_{Q2}))$, the basin of attraction of Q_1 being $(0, \xi_{Q2})$ (see Fig. 15(a), for $p = 0.63$).

The two cycles C_1 and C_2, merging at the bifurcation value $p = p_1$, separate more and more as p increases. As a consequence, the region of the phase space whose points are convergent to the limit cycle C_1 increases. C_1 persists, stable, for a wide range of p values, but the slope of the map g at

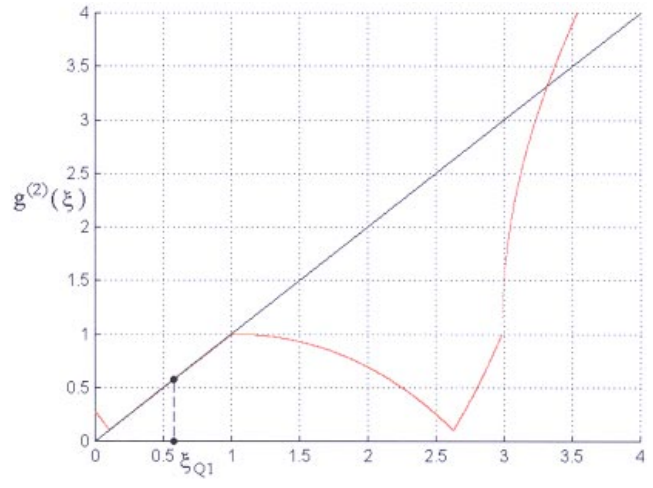

Fig. 18. The map $g^{(2)}$ for $p = q = 1.5$ (nonstandard bifurcation of the fixed point Q_1).

the point Q_1 becomes negative and approaches the bifurcation value -1. This happens at $p = q = 1.5$ through a nonstandard "flip bifurcation" of Q_1. As a matter of fact, it can be proved that, for $p = q$, there exist a whole interval of ξ values in which $dg/d\xi = -1$. Such an interval can be more easily observed on the graph of the map g^2; a whole segment of the bisectrix line belongs to the graph of g^2, as shown in Fig. 18. It is evident that, at the bifurcation value $p = q$, infinite pairs of symmetric limit cycles exist in the flow. Even if such cycles are not asymptotically stable, they attract all the nondivergent trajectories, except for the one coincident with C_2.

Soon after the bifurcation value, for p slightly larger than q, the limit cycle C_1 becomes unstable, and its stable manifold separates two regions, each containing an attractive set. Such a bifurcation generates two disjoint and symmetric chaotic attractors. In the phase space, the two attractors lie one "below" and the other "above" C_1. The basins of attraction of the two chaotic attractors

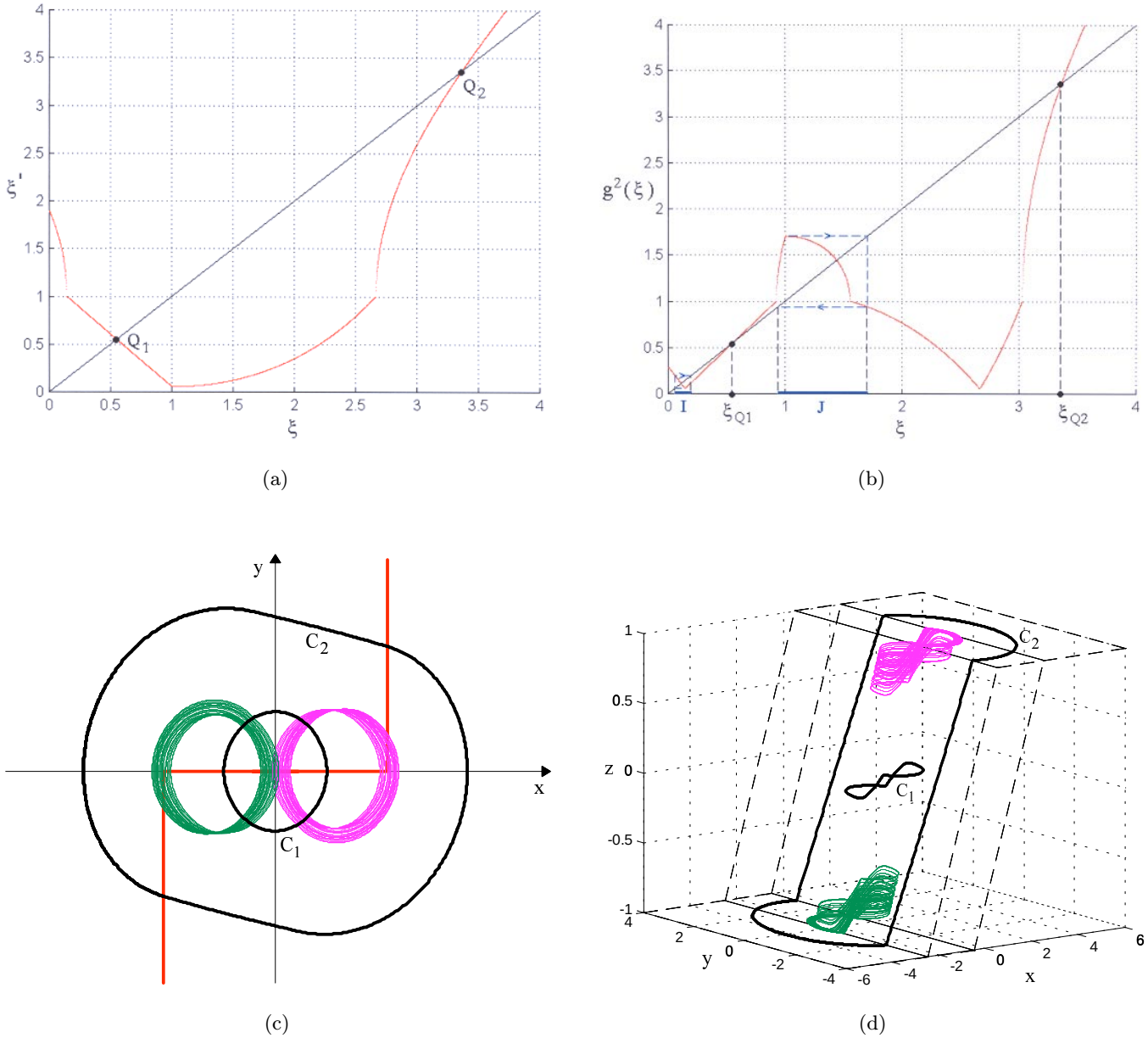

(a) (b) (c) (d)

Fig. 19. The maps (a) g and (b) $g^{(2)}$ (with invariant intervals) for $p = 1.55$; corresponding disjoint symmetric chaotic attractors and limit cycles C_1 and C_2 (both unstable) (c) on the (x, y) plane and (d) in the (x, y, z) space.

in the flow are separated by the stable manifold of C_1, while the stable manifold of C_2 still separates the divergent flow from the flow eventually trapped within one or the other of the two attractors. In other words, the flow enters a "well-known" (for this kind of flows) regime of bistability. This can be explained by looking at the map g^2, for instance, in Fig. 19 (for $p = 1.55$), where two stable invariant intervals, I and J, can be seen, one to the right and the other to the left of Q_1. In the proposed example and for many other values of q, the dynamics inside these intervals has been observed to be chaotic. However, for some values of q, the attractors in these intervals might be stable fixed points corresponding to stable 2-cycles of g (flip-bifurcated from Q_1).

The coexisting attractors in the flow are shown in Figs. 19(c) and 19(d). The green plot is the attractor which corresponds to the left invariant interval, I, in Fig. 19(b), and the magenta plot corresponds to the flow in the right invariant interval, J, in the same figure.

The system exhibits "uncertainty" with respect to initial conditions close to (and lower than) ξ_{Q2} in

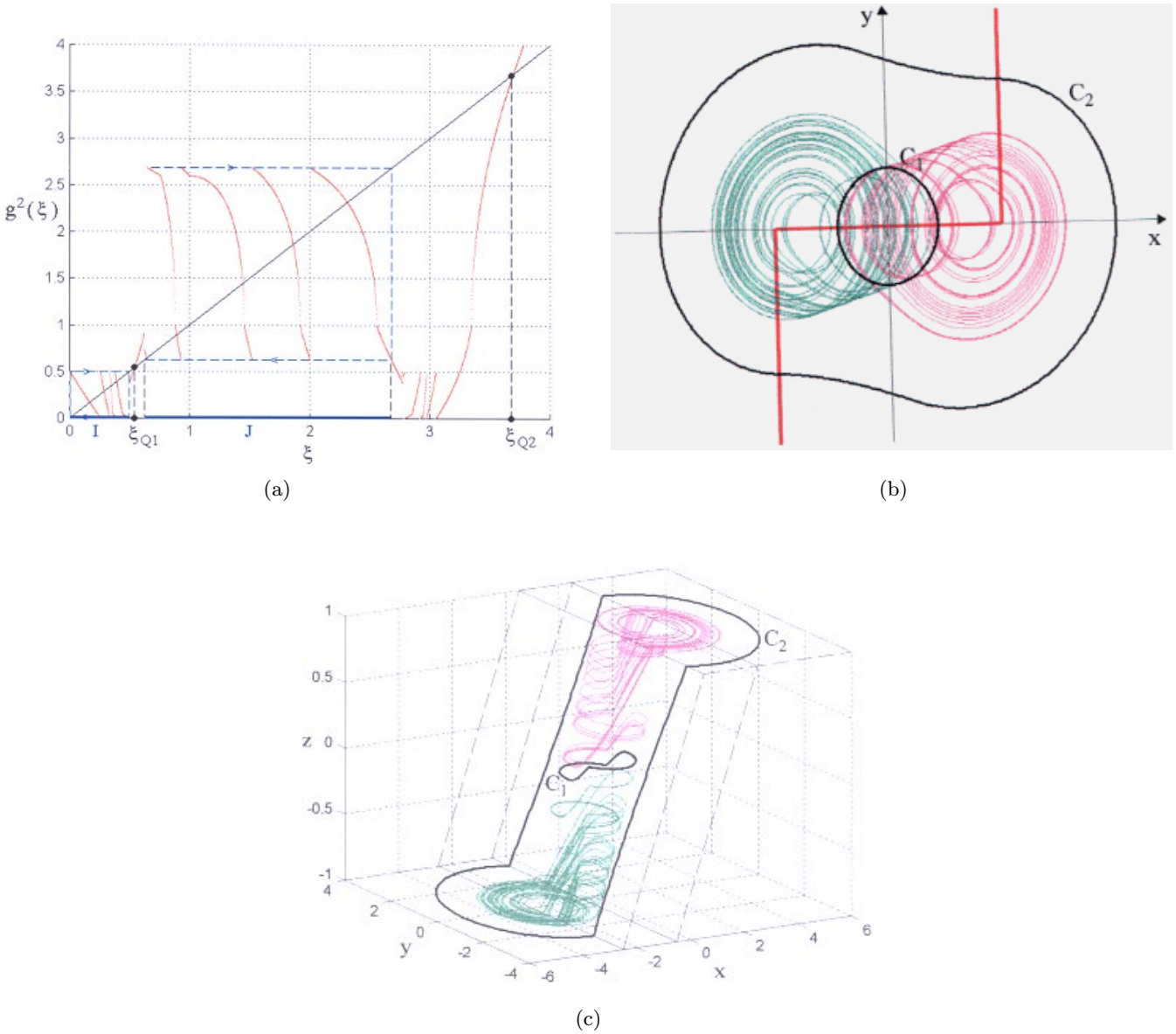

Fig. 20. (a) The map $g^{(2)}$ (with invariant intervals) for $p = 2$; corresponding disjoint symmetric chaotic attractors and limit cycles C_1 and C_2 (both unstable) (b) on the (x, y) plane and (c) in the (x, y, z) space.

the map g. This means that, for initial conditions close to the boundary of the space of divergent trajectories (i.e. close to the unstable limit cycle C_1 and to its stable manifold), it is difficult to predict the asymptotic state.

In the example shown in Fig. 19, one can easily identify two fixed points of g^2 that are not fixed points of g and that correspond to unstable limit cycles in the flow (an example is given in Fig. 14). Many other k-cycles in the flow exist that correspond to fixed points of g^k $(k > 2)$ that are not fixed points of g^h $(1 < h < k)$.

To sum up, for several values of q, when p increases after q, one can observe a pair of nonsymmetric chaotic attractors, as shown in Fig. 20 (for $p = 2$).

Note that the number of discontinuities in the map g grows until p reaches the value $q + 1$ (at this

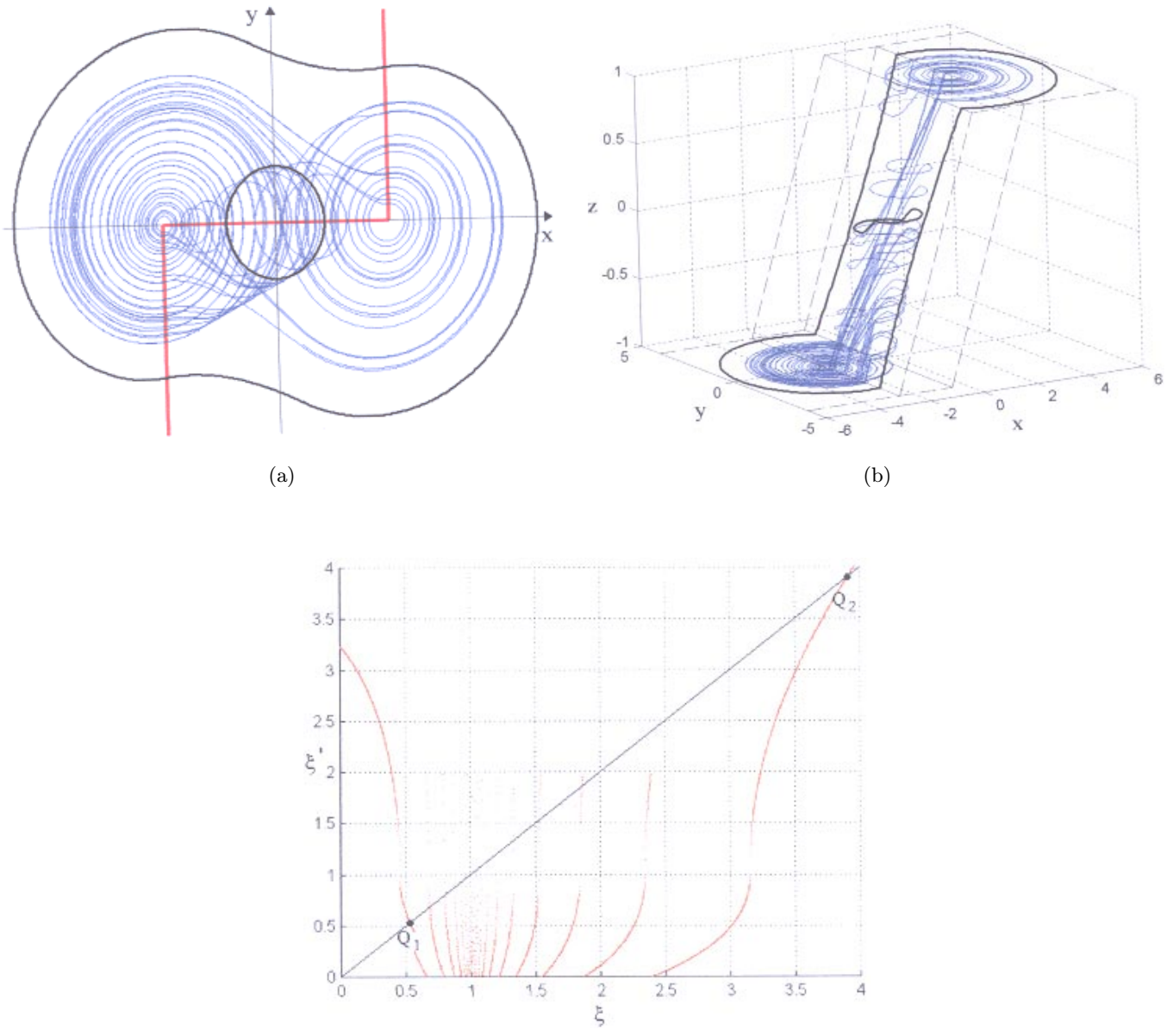

Fig. 21. Merged chaotic attractor, and limit cycles C_1 and C_2 (both unstable), (a) on the (x, y) plane and (b) in the (x, y, z) space, for $p = 2.49$; (c) the corresponding map g.

value of p, the equilibrium points P_{DB} and P_{AB} lie at the vertices of Γ and Γ', respectively); then such a number decreases.

From Fig. 20, one can easily see that, as p is increased, the two chaotic attractors (and, correspondingly, the two stable invariant intervals I and J in the map g^2) approach each other and, at the same time, they approach the limit cycle C_1 (ξ_{Q1} in the map g^2).

As p is further increased, we encounter another interesting bifurcation marking the merging of the two chaotic attractors into a single (chaotic) attractor (in our example, this occurs for $p = p_2 \cong 2.05$). In g, such a bifurcation takes place when the two invariant intervals I and J of g^2 become wide enough to touch the fixed-point abscissa ξ_{Q1}, thus determining [Mira *et al.*, 1996] the first homoclinic bifurcation of Q_1 and, likewise, of the periodic orbit C_1 in the flow. As a matter of fact, the stable and unstable manifolds of C_1 have a contact, then they intersect. An example of trajectory of the merged attractor, exhibiting a typical "double-scroll" form, is given in Figs. 21(a) and 21(b) for $p = 2.49$. Figure 21(c) shows the related map, where it is easy to

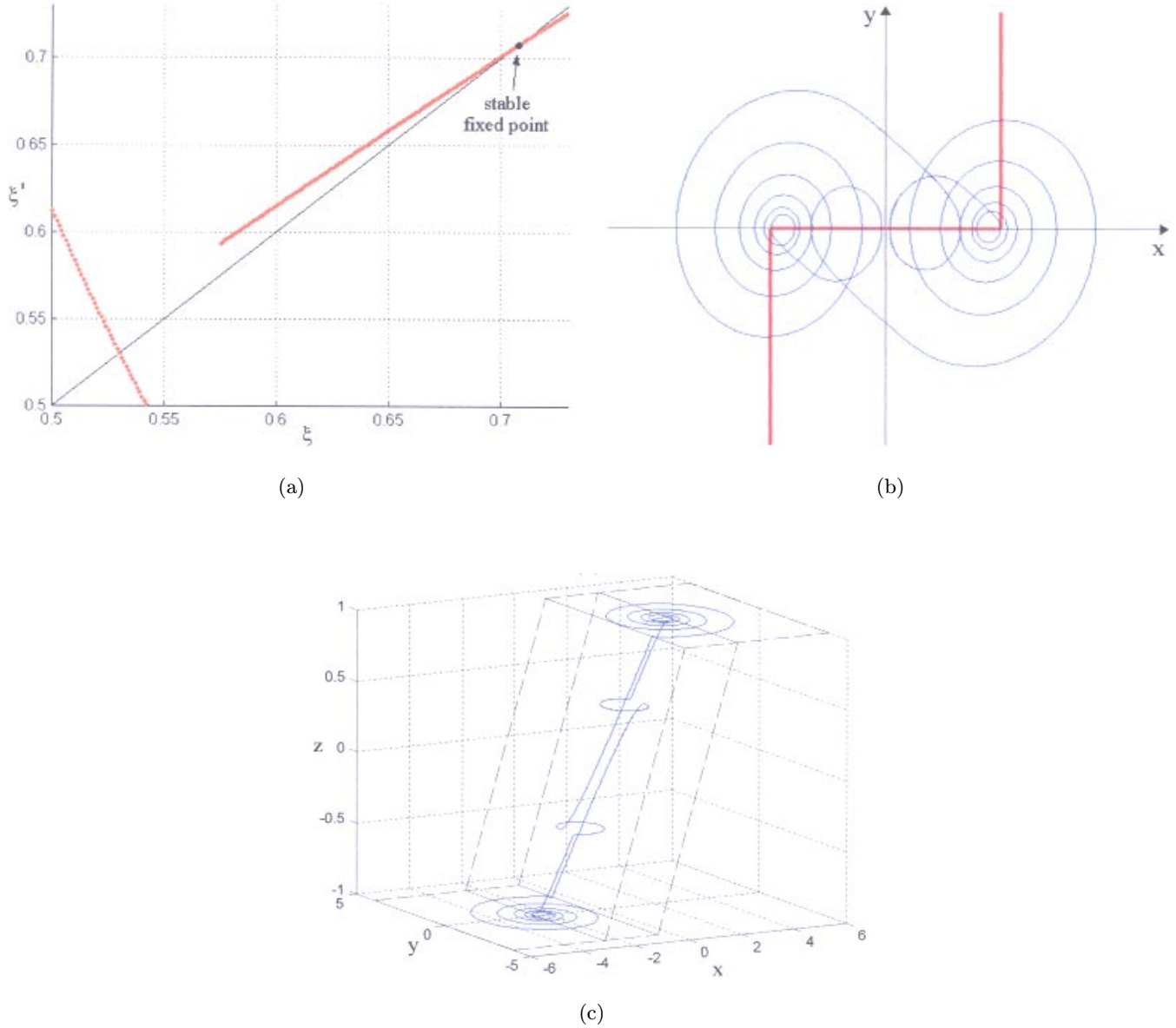

Fig. 22. (a) The map g for $p = 2.288$ (zoom), (b) asymptotic limit cycle on the (x, y) plane and (c) in the (x, y, z) space.

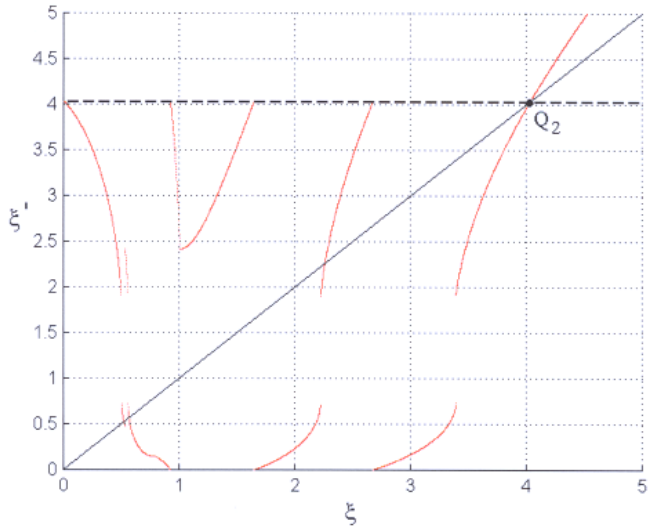

Fig. 23. The map g for $p = 3.47$.

draw homoclinic points to Q_1 and to desume that the number of discontinuities tends to ∞.

Although, for $p > q$, the dominant regime is chaotic, there exist several narrow windows of p values corresponding to either a stable symmetric limit cycle or a symmetric pair of stable limit cycles. This fact is related to the existence of a stable fixed point of either g or g^k $(k > 1)$, which often exist even in the chaotic regime. We remark that, as infinitely many unstable cycles still exist and belong to the basin boundary, the basin turns out to have a fractal structure [Mira *et al.*, 1996]. In such a regime, eventually periodic trajectories are preceded by long chaotic transients. An example is presented in Fig. 22, for $p = 2.288$. The tangent (or fold) bifurcation of g shown in Fig. 22(a) (or, generally speaking, those of its kth iteration g^k $(k > 1)$) is related to the existence of a limit cycle in the flow [see Figs. 22(b) and 22(c)].

The end of the observable bounded dynamics is reached at a final value $p = p_3 \cong 3.47$, such that $g(0; p_3) = \xi_{Q2}$ (see Fig. 23). For $p > p_3$, the bounded invariant set of g (and of the flow) becomes a fractal repeller, and the generic trajectory (in both the map g and the flow) is divergent.

5. Concluding Remarks

A one-dimensional map g has been used as a tool for the analysis of the PWL flow associated with a nonlinear oscillator based on hysteresis. The main bifurcations occurring in the dynamics of the circuit by varying the parameter p and several regular and chaotic behaviors have been illustrated. The predominant regime in the circuit dynamics results in being chaotic and two types of strange attractors, corresponding to different asymptotic flows, have been found. In particular, there exists a p value, which marks the transition (homoclinic bifurcation) from the presence of two symmetric coexisting chaotic attractors (corresponding to a regime of bistability) to a "double-scroll"-like one.

Acknowledgments

This work was supported by the Ministero dell'Università e della Ricerca Scientifica, Rome, within the framework of the research project "Neural and nonlinear circuits for one- and multidimensional signal processing applications."

References

Alligood, K. T. & Sauer, T. D. [1997] *Chaos: An Introduction to Dynamical Systems* (Springer-Verlag, NY).

Kennedy, M. P. & Chua, L. O. [1991] "Hysteresis in electronic circuits: A circuit theorist's perspective," *Int. J. Circuit Th. Appl.* **19**, 471–515.

Lupini, R., Bizzarri, M. & Storace, M. [2001] "Discontinuities in a one-dimensional map describing a hysteretic chaotic circuit," *Nonlinear Analysis — Theory, Methods & Applications*, to be published.

Mira, C., Gardini, L., Barugola, A. & Catala, J. C. [1996] *Chaotic Dynamics in Two-Dimensional Noninvertible Maps* (World Scientific, Singapore).

Nakagawa, S. & Saito, T. [1996] "An RC OTA hysteresis chaos generator," *IEEE Trans. Circuits Syst.* **43**, 1019–1021.

Parodi, M., Storace, M. & Cincotti, S. [1994] "A PWL ladder circuit which exhibits hysteresis," *Int. J. Circuit Th. Appl.* **22**, 513–526.

Parodi, M., Storace, M. & Cincotti, S. [1996] "Static and dynamic hysteretic features in a PWL circuit," *Int. J. Circuit Th. Appl.* **24**, 183–199.

Storace, M. & Parodi, M. [1998] "Simple realisation of hysteresis chaos generator," *Electron. Lett.* **34**, 10–11.

Storace, M., Parodi, M. & Robatto, D. [1999] "A hysteresis-based chaotic circuit: Dynamics and applications," Special Issue: Communications, Information Processing and Control Using Chaos, *Int. J. Circuit Th. Appl.*, eds. Hasler, M. & Vandewalle, J. **27**, 527–542.

Strogatz, S. H. [1994] *Nonlinear Dynamics and Chaos* (Addison-Wesley, Reading-MA).